Crystalline intermetallic compounds in the K-Te system: The Zintl-Klemm principle revisited

Karin Seifert-Lorenz and Jürgen Hafner

Institut für Materialphysik and Center for Computational Material Science, Universität Wien, Sensengasse 8, A-1090 Wien, Austria

We have investigated the crystal structure, chemical bonding, and electronic properties of all known intermetallic compounds in the K-Te system, employing a first-principles local-density-functional approach including generalized gradient corrections. The structural parameters, such as equilibrium volume, lattice constants, and internal parameters are in very good agreement with experiment. The evaluation of the total and angular-momentum decomposed densities of states (DOS) and the partial charge densities gives further insight into the bonding properties of these solids. Our results confirm the validity of the Zintl-Klemm principle for the saltlike compound K_2Te and for the two equiatomic phases α-K_2Te_2 and β-K_2Te_2 consisting of isolated K ions and covalently bounded Te_2 dimers. In the compound K_5Te_3 ionic regions consisting of K^+ and Te^{2-} ions with closed octet shells and polyanionic regions with an atomic arrangement dominated by Te_2^{2-} dianions coexist in the crystal lattice. In the electron-deficient-compound K_2Te_3, larger polyanions—Te_3^{2-} trimers—have to be formed to achieve saturated covalent bonds. Our results illustrate the validity and astonishing flexibility of the Zintl-Klemm principle, which allows us to interpret all crystal structures in the K-Te system , from the saltlike octet compound to the Te-rich phases with extended polyanionic superstructures, on a common footing.

I. INTRODUCTION

The properties of tellurides vary in a wide range from saltlike compounds over semiconducting compounds with strong covalent Te-Te bonding to metallic character. This different behavior reflects the possibility of the heavy chalcogen atom to build more than two bonds, unlike sulfur and also selenium, which usually behaves in polychalcogenes like sulfur. The structural and physicochemical properties of a large number of compounds of alkali and alkaline-earth metals with polyvalent elements from groups III to VI, the so-called Zintl phases, can be explained by a picture originally proposed by Zintl and co-workers,[1,2] Hückel,[3] and Hewaidy *et al.*[4] In a compound of an alkali-metal or alkaline earth metal *A* with a polyvalent metal or semimetal *M*, the electropositive element transfers its valence electron(s) to the electronegative partner. If the charge transfer leads to a complete octet shell of the electron acceptor, a saltlike compound is formed, e.g., K_3Sb or K_2Te. In accordance with the band-filling model for the metal-nonmetal transition, the octet compounds are narrow-gap semiconductors. At lower electron-donor concentrations, the charge transfer is not sufficient to complete the octet shell of the acceptor. A saturated chemical bond between the polyvalent atoms can be achieved only by sharing valence electrons among the anions, leading to the formation of polyanionic clusters or sublattices. If one electron is transferred to the acceptor, its real environment will be similar to the elements to its right in the periodic table of the elements. Examples are tetrahedral M_4^{4-} polyanions in I-IV alloys, such as KSn or CsPb, forming a structure well known from white phosphorus or arsenic in the gas phase,[5] or infinite helical $(Sb^-)_\infty$ chains in KSb, similar to those in trigonal Se or Te (Ref. 6). Generally, these compounds obey a modified octet rule

$$b = 8 - n_{VA}, \qquad (1)$$

where b is the number bonds per atom and n_{VA} the number of valence electrons per electron acceptor. As long as n_{VA} is a natural number, two electrons per covalent bond between two anions are available, and these alloys are referred to as Zintl-Klemm compounds. Additionally, a variety of electron-deficient compounds exist, in which the bonding electrons are distributed over more than two atom centers. An example is the compound K_8Tl_{11}, forming $(Tl_{11})^{8-}$ clusters.[7] There are also phases intermediate between the octet compounds and the classical polyanionic structures. In K_5Sb_4 for example, the excess electron due to the higher *K* content leads to a disruption of the infinite $(Sb^-)_\infty$ chains into $(Sb_4)^{5-}$ tetramers in which the dangling bonds at the chain ends are at least partially saturated by the excess electrons.[6] For an overview of the wide field of Zintl phases, their structures and bonding mechanisms, see, e.g., Refs. 8 and 9.

The Zintl-Klemm principle requires the formal charge transfer of *all* the valence electrons from the electropositive to the electronegative element. The fact that early electronic structure calculations indicated that the actual charge transfer is small has lead to a widespread critique of the Zintl model.[10–12] However, it has now become clear that charge transfer (a quantity that is notoriously difficult to define and to determine in a quantitative way) is not the distinguishing feature of Zintl alloys. In fact, the behavior of the electrons are governed by the strongly attractive electron-ion potential of the electronegative element. Various band structure calculations show that the valence rule still applies, because one has to count occupied bands rather than local charges.

The calculation of the band structure of I-IV compounds shows a striking similarity with the term scheme of P_4 or As_4 molecules,[13–15] and likewise the density of states of equiatomic compounds in the I-V systems is characterized by the same tripartite bonding, nonbonding, and antibonding structure found in the chalcogen elements Se and Te.[6,16,17] These calculations show that the Zintl principle is valid, as long as one thinks in terms of molecular orbitals and not of localized charges.

The Zintl-Klemm principle explains the mechanism leading to polyanionic clustering. In addition the chemical stability of the clusters is strongly influenced by the volume of the alkali metal separating these clusters. It can be seen as a general rule that the larger the donor atoms, the more stable the Zintl ions.

The intimate connection between electronic and atomic structure holds not only in the solid but also in the liquid (as shown by various neutron- and x-ray-scattering experiments[18,19]), establishing the stability and flexibility of the polyanionic bonds postulated by the Zintl-Klemm principle. A proof of the conjecture that this principle does indeed explain the structure and stability of such a wide class of intermetallic compounds can be delivered by self-consistent calculations of the atomic and electronic structure in both phases. Modern total-energy calculations using density-functional techniques allow us to perform an optimization of the crystal structure with respect to all parameters (and, in the liquid phase, even to perform *ab initio* molecular dynamics simulations of the structure of the melt). For the optimized structure, the electronic spectrum and electron-density distributions may be analyzed and the character of the interatomic bonding can be determined. This approach to the atomic and electronic structure and of the stability in the solid and the liquid phases simultaneously was already successfully applied to the K-Sb system[6,20] and the alkali-metal–tin system.[21–24]

The present work is devoted to the K-Te system. There are several reasons why the potassium tellurides are of special interest. First of all, the structures of the octet compound K_2Te (Ref. 25) and the equiatomic compound K_2Te_2 (Ref. 25 and 26) are rather simple: K_2Te is a typical saltlike octet compound and isolated Te^{2-} anions are separated by K^+ cations. K_2Te_2 exists in two different modifications: the low-temperature phase α-K_2Te_2 and the high-temperature phase β-K_2Te_2. Both obey the Zintl-Klemm rule and are built of $(Te_2)^{2-}$ dianions. This simplicity of the crystal structures allows us to study the basic bonding mechanism. In addition to these "stoichiometric" compounds two stable intermediate phases, K_2Te_3 (Ref. 27) and K_5Te_3 (Ref. 28), exist, allowing us to study the more complicated electronic structure and chemical properties of electron-deficient and excess-electron Zintl compounds. In the tellurium-rich phase K_2Te_3 $(Te_3)^{2-}$ trimers have been identified. The structure of the potassium-rich phase K_5Te_3 is rather complex, involving direct K-K bonds so that the Zintl principle alone is not sufficient for understanding structure and bonding.

In the present work, we present a detailed study of the crystalline and electronic structures of all four K-Te compounds using first-principles density-functional techniques. In a subsequent paper these investigations will be extended to the liquid K-Te alloys, using *ab initio* density-functional molecular dynamics.

II. COMPUTATIONAL METHODS

All our calculations are based on local density-functional theory (DFT) and the pseudopotential method, using the Vienna *ab initio* simulation package (VASP). VASP employs a

TABLE I. Equilibrium atomic Ω, nearest-neighbor distances d, cohesive energies E, and bulk modulus B of trigonal Te and body-centered-cubic K as calculated in the local density (LDA) and generalized gradient (GGA) approximations, compared to experiment.

		Ω (Å^3)	d(Å)	E(eV)	B(GPa)
Te	Expt.[a]	33.891	2.832	−2.23	19.4,18.7
	LDA	31.407	2.906	−3.797	33.9
	GGA	34.998	2.892	−3.156	18.8
K	Expt.[b]	75.710	4.614	−0.934	3.7
	LDA	64.884	4.384	−1.130	4.3
	GGA	73.956	4.580	−1.030	3.4

[a]After Ref. 35. The bulk modulus quoted here has been calculated from a Murnaghan fit to the published equation of state.
[b]After Ref. 34.

plane-wave expansion of the valence states and a description of the ion-electron interaction in terms of ultrasoft pseudopotentials (PP).

A question always arising in DFT is the choice of the exchange-correlation functional. Today modern generalized gradient approximations (GGA) have superceded the local density approximation (LDA). This is also confirmed by our calculations: for both elements the LDA calculations always lead to a substantial underestimate of the equilibrium volume compared to the experimental one (see Table I). For K (like for all alkali metals), the GGA reduces the LDA error in the prediction of the equilibrium volume from 14% to about 2%. For Te, the GGA corrections overshoot and lead to an atomic volume that is about 3% too large. It has to be emphasized that both LDA and GGA lead to almost the same interatomic distances along the Te chains, but differ strongly in the interchain distances. Both the LDA and the GGA underestimate the ratio d_2/d_1 between the inter- and intrachain distances, overestimating the distances along the chains, but underestimating the distances between the neighboring chains. However, the GGA is much closer to experiment. For a detailed discussion of the crystal structure of Te as described by GGA and LDA, we refer to the paper of Kresse *et al.*[16] However, it has to be pointed out that the GGA functional chosen here leads to even better agreement with experiment than the Perdew-Becke functional used earlier. In summary, the gradient-corrected functionals are much more appropriate for the compounds. Hence we present only the GGA results, obtained using the PW91 functional of Wang and Perdew.[29]

A fully nonlocal ultrasoft pseudopotential was constructed according to the prescription of Vanderbilt[30] as modified by Kresse and Hafner.[31] Two energy channels were used for the s and p wave functions, and the cutoff radii for the wave functions were $R_{c,Te}=1.37$ Å and $R_{c,K}=2.03$ Å and for the augmentation charge $R_{aug,Te}=1.53$ Å and $R_{aug,K}=2.28$ Å, respectively. For both elements a norm-conserving d-electron pseudopotential was chosen as local potential.

The Hellmann-Feynman theorem allows the calculation of the forces acting on the ions from the ground state of the electronic system. To find the energy minimum of the ionic

TABLE II. Atomic structure and cohesive properties of crystalline CaF_2-type K_2Te as calculated in the GGA, compared to experiment.

Pearson symbol $cF16$, space group $Fm\bar{3}m$	GGA	Expt.[a]
Atomic volume Ω_0 ($Å^3$)	46.498	45.079
$\Delta\Omega$ (%)	3.1	
Excess volume $\Delta\Omega_{ex}$ (%)	-23.74	-27.02
Lattice parameter a(Å)	8.233	8.148
Cohesive energy (eV/atom)	-2.804	
Heat of formation ΔH (eV/at)	-1.064	
Bulk modulus B(Mbar)	12.9	
$\partial B/\partial P$	4.3	
Nearest-neighbor distances		
$d_{K\text{-}K}$ (Å)	4.116	4.074
$d_{K\text{-}Te}$ (Å)	3.565	3.528
$d_{Te\text{-}Te}$ (Å)	5.821	5.762

[a]After Ref. 34.

system a conjugate-gradient algorithm[32] is used. All atomic degrees of freedom, the volume and shape of the unit cell, and the internal positions of the atoms, are relaxed simultaneously, subject only to the constraint of maintaining space-group symmetry. Additionally a series of calculations at different fixed volumes was performed to calculate the bulk modulus and to determine the variation of the crystal structure under pressure. The bulk modulus has been determined by a least-squares fit of the volume-energy and volume-pressure data to a Murnaghan equation of state.

Once the atomic positions and the pseudo-wave-functions have been calculated we employ various tools to analyze the data. The atomic structure is discussed in terms of the calculated lattice parameters, atomic positions, interatomic distances, bonding angles, etc. Calculation of the excess volume and heat of formation leads to information about the stability of the crystalline phases.

The electronic eigenstates in **k**-space are characterized by the band structure and its **k**-space integral—the density of states (DOS). An important step towards a real-space descriptions are the partial or local DOS (LDOS), calculated by projecting the plane waves representing the eigenstates onto spherical harmonics within spheres centered at the atom sites (for detailed description see Ref. 33). In addition, the electron-density distributions corresponding to certain groups of bands can be used to characterize the chemical bonding.

III. THE OCTET COMPOUND K_2Te

A. Atomic structure

K_2Te crystallizes in the face-centered-cubic (fcc) CaF_2 structure (space group $Fm\bar{3}m$) with 12 atoms in the conventional unit cell.[34] The Te atoms are located at the Wykoff position $4a$, (0,0,0), and the K atoms at positions $8c$, $(\frac{1}{4},\frac{1}{4},\frac{1}{4})$, filling the octahedral holes.

Table II shows the results of our calculations compared with experiment. The volume is a bit overestimated (the error
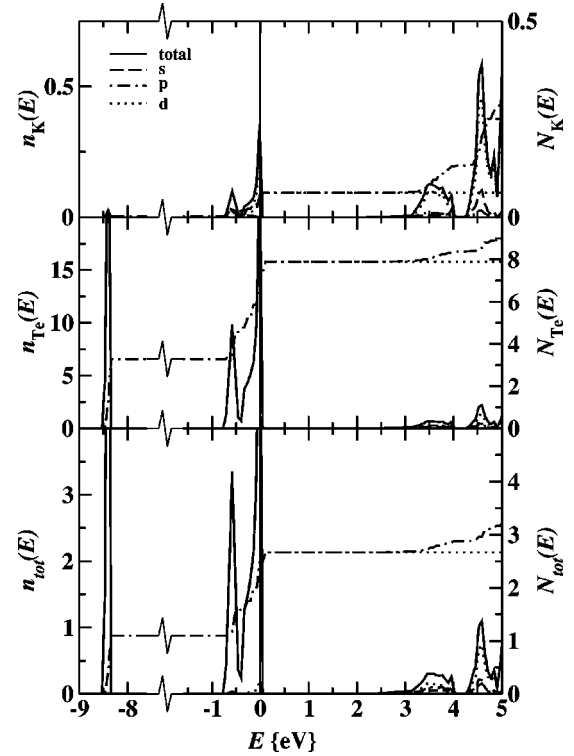
FIG. 1. (a) Total and local angular-momentum-decomposed electronic density of states in K_2Te with the CaF_2 structure. The right-hand scale shows the integrated density of states.

is of the same order of magnitude as for pure Te), the excess volume is very large and negative ($\Delta\Omega_{ex}=-24\%$), but the experimentally observed contraction ($\Delta\Omega_{ex}=-27\%$) is still underestimated. The volume contraction of almost 30% is almost entirely due to a compression of the K atom: Compared to the interatomic K-K distances in pure potassium (see Table I), the K-K distance in the alloy is reduced by 11.1%. This means a contraction of 30% of the potassium atom and is an indication for the ionic character of the bonding. This is also supported by the K-Te distance $d_{K\text{-}Te}=3.528$ Å, which is close to the sum of the Pauling ionic radii $R_{K^+}+R_{Te^-}=1.33$ Å$+2.21$ Å$=3.51$ Å, whereas adding up the covalent radii will underestimate the distance. The calculated bulk modulus is about four times larger than that in pure potassium, but just a few GPa lower then in t-Te. As the structure and the bonding properties are not determined by Te-Te bonding, this is most likely coincidental. More important seems to be the finding that the bulk modulus is almost the same as in K_3Sb, the octet compound in the K-Sb system.[6]

B. Electronic structure

In Fig. 1 the total and angular-momentum-decomposed DOS's are shown. The calculation of the LDOS was performed using the Pauling ionic radii ($R_{K^+}=1.33$ Å, $R_{Te^-}=2.21$ Å) to define the projection spheres.

The electronic structure confirms the picture of a saltlike ionic compound: The lowest valence band is a narrow Te s band; the two highest occupied bands have Te p character.
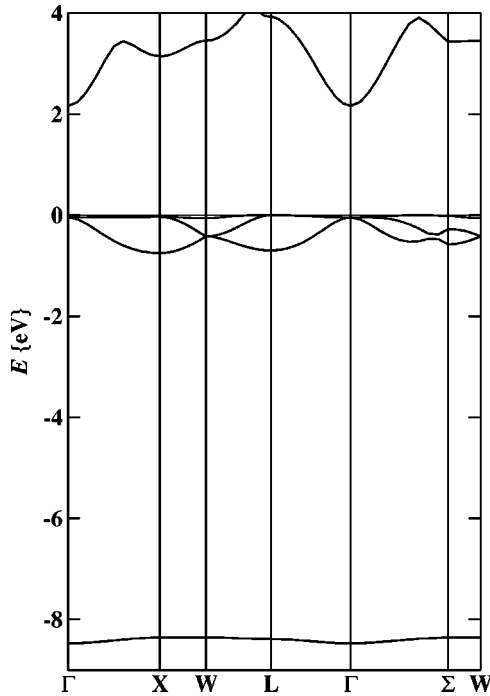
FIG. 2. Electronic band structure of K_2Te along the principal symmetry lines.

The local DOS at the K sites shows a strongly mixed s, p, d character, indicating that the DOS represents mainly states centered at the Te sites overlapping onto the K spheres. The integration of the local DOS at the different sites shows almost a complete charge transfer from the alkali metal to the polyvalent Te, confirming the Zintl picture. It must be stressed, however, that the local charges depend strongly on the radii of the projection spheres. The lowest conduction band is dominated by unoccupied K states. The high electronic pressure caused by the strong volume contraction at the K sites leads to a lowering of the local d states compared to the delocalized s states; hence the conduction band shows a distinctly mixed s-d character.

These features are also confirmed by the dispersion relations of the electronic eigenstates as shown in Fig. 2. K_2Te is an insulator with an indirect gap $L \rightarrow \Gamma$ of 2.16 eV; the direct gap at the Γ point is only a few hundreds of an eV wider. In contrast to the highest Te valence band, which is almost dispersionless, the lowest unoccupied K conduction band shows strong dispersion around Γ, giving only a small contribution to the DOS. This leads to a tail at the low-energy edge of the conduction states, similar to that discovered in the alkali-metal pnictide compounds in the BiF_3 structure, and a substantially wider gap of ~ 3 eV seen in the DOS (Fig. 1) and detectable in optical experiments.[6,36]

IV. THE EQUIATOMIC COMPOUND K_2Te_2

The compound K_2Te_2 exists in two modifications: a low-temperature phase called α-K_2Te_2 and a high-temperature phase β-K_2Te_2. The $\alpha \rightarrow \beta$ transition takes place at ~ 510 K, and the melting point of the β phase is about 660 K (Refs. 26 and 37).

TABLE III. Equilibrium volume and lattice parameters of α-K_2Te_2 and β-K_2Te_2 compared to experimental data.

System		a	c	c/a	Ω	$\Delta\Omega$	$\Delta\Omega_{ex}$
α-K_2Te_2	VASP	9.6637	6.4781	0.6704	43.66	2.8%	-19.9%
α-K_2Te_2	Expt.[a]	9.5140	6.5000	0.6832	42.46	—	-22.5%
β-K_2Te_2	VASP	5.6543	12.3386	2.1822	42.70	3.6%	-21.6%
β-K_2Te_2	Expt.[a]	5.5890	12.1880	2.1807	41.21	—	-24.8%

[a]Reference 26.

A. Atomic structure

1. Atomic structure of α-K_2Te_2

α-K_2Te_2 crystallizes in the Na_2O_2 structure.[26,37] The characteristic elements of this structure are dichalcogen dumbbells parallel to the c axis. They form infinite straight chains with alternating short distances within the dumbbells and long distances between two neighboring dumbbells. The formation of Te_2 dumbbells confirms the Zintl rule: Due to the charge transfer from the alkali metal to the chalcogen, Te^- becomes isoelectronic to the halogen atoms, forming dimers to complete an octet shell. Hence it is more appropriate to talk about Te_2^{2-} dianions instead of neutral Te_2 molecular units.

The space group of this structure is $P\bar{6}2m$ with three formula units per hexagonal cell: K_6Te_6. Alkali and chalcogen atoms each occupy two crystallographically inequivalent sites: K1 at $3f$, $(x_1,0,0)$, with $x_1 \approx \frac{2}{3}$ and K2 at $3g$, $(x_2,0,\frac{1}{2})$, with $x_2 \approx \frac{1}{3}$, as do the chalcogen atoms Te1 at $2e$, $(0,0,z_1)$, with $z_1 \approx 0.2$ and Te2 at $4h$, $(\frac{1}{3},\frac{2}{3},z_2)$, with $z_2 \approx 0.3$. There are two pseudo-sum-rules: $x_1 \approx -x_2$ and $z_2 \approx \frac{1}{2} - z_1$. Changing internal parameters such that all nearest-neighbor Te-Te distances are equal would lead to the LiAs-crystal structure with -Te-Te-Te- chains.

In Table III the volume and lattice parameters of α- and β-K_2Te_2 are given, and agreement with experiment is satisfactory for both modifications. The volume of α-K_2Te_2 is overestimated by 2.8% and the large experimental excess volume is slightly underestimated. The variation of the lattice parameters a and c with volume is shown in Fig. 3(b). As the lattice parameters increase both linearly with increasing volume, the ratio c/a is constant from $\Omega \simeq 36$ Å^3 to $\simeq 44$ Å^3.

In Table IV the free parameters determining the atomic positions and the resulting interatomic distances are given. For the K atoms the pseudo-sum-rule $x_1 \approx -x_2$ is fulfilled a bit better by the calculated parameters than for the experimental ones. The change in the positions of the K atoms leads to a more symmetric arrangement of the K atoms around the Te-Te dumbbells and hence to almost identical interatomic distances $d_{K-Te1} \simeq d_{K-Te2}$.

The structure of α-K_2Te_2 can be described as hexagonal channels built of K-atoms parallel to the c axis centered by the Te_2^{-2} dianions. Projected on the xy plane the structure looks like a honeycomb lattice, each corner of the hexagons being occupied by a K atom, every second lying in one plane, the other three in a parallel plane shifted at $c/2$ to
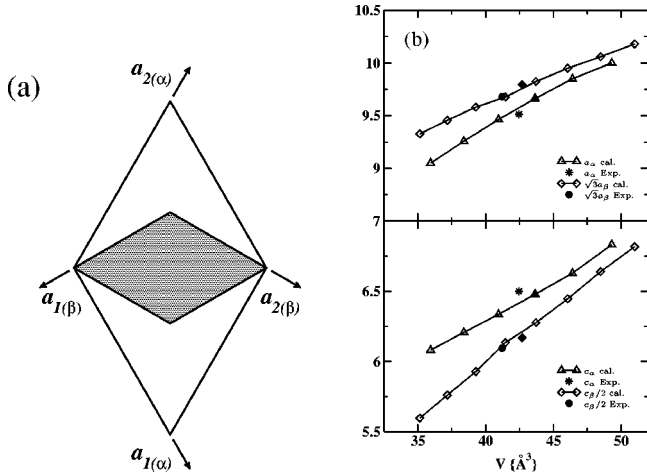
FIG. 3. (a) Metric relationship between the unit cells of α- and β-K_2Te_2 and (b) variation of the cell parameters a and c for both modifications over volume: Triangles mark the calculated cell parameters of α-K_2Te_2, diamonds those of β-K_2Te_2, the filled symbols refer to the fully relaxed structure at equilibrium volume, and the stars and the filled circle stand for experimental parameters of the α and β phase, respectively.

build up infinite tubes. The calculated internal lattice parameters lead to an almost regular hexagonal pattern, the experimental data to a slightly distorted arrangement. There seems to be no reason why positions leading to a lower symmetry (not in terms of the crystal structure, but in terms of bonding lengths) would be preferred. As the experimental structure parameters were obtained by x-ray diffraction experiments[37] the contributions from the Te atoms are about 8 times larger than those from the potassium atoms. This seems to be a good reason to think the calculated parameters are reliable.

TABLE IV. Internal parameters and interatomic distances in α-K_2Te_2 compared to experimental data.

	Internal parameters			
	x_1	x_2	z_1	z_2
VASP	0.6558	0.3218	0.2187	0.2802
Expt.	0.6700	0.3000	0.2200	0.2800

	Interatomic distances (Å)			
	d_{K1-K1}	d_{K1-K2}	d_{K2-K2}	
VASP	4.570	4.573	5.386	
Expt.	4.428	4.791	4.944	

	d_{K1-Te1}	d_{K1-Te2}	d_{K2-Te1}	d_{K2-Te2}
VASP	3.615	3.653	3.604	3.574
Expt.	3.450	3.670	3.385	3.634

	$d_{Te1-Te1}$	$d_{Te1-Te1}$	$d_{Te2-Te2}$	$d_{Te2-Te2}$
VASP	2.833	3.645	2.847	3.631
d_2/d_1	1.000	1.287	1.000	1.275
Expt.	2.860	3.640	2.860	3.640
d_2/d_1	1.000	1.273	1.000	1.273

The pseudo-sum-rule concerning the positions of the Te atoms, $z_2 \approx \frac{1}{2} - z_1$, is satisfied by the experimental values exactly, leading to identical Te-Te distances within the dumbbells as well as between them for the Te1 and Te2 atoms. The calculated $d_{Te1-Te1}$ and $d_{Te2-Te2}$ distances differ slightly, as there is no symmetry constraint to give exactly the same distances, but the difference is very small (less then 0.02 Å), so the positions of the Te atoms within the unit cell are very well reproduced.

The volume dependence of the Te-Te distances is shown in Fig. 4(a). Whereas the length of the Te_2^{2-} dumbbells remains almost unchanged with decreasing volume, the distances between the dianions scale linearly with the lattice parameter c, indicating that the bonding between the dumbbells is rather weak.

2. Atomic structure of β-K_2Te_2

β-K_2Te_2 crystallizes in the Li_2O_2 structure type[26,37]. This structure also obeys the Zintl principle, as the main elements of the lattice are again $(Te_2)^{2-}$ dumbbells. The Li_2O_2 structure has space group $P6_3/mmc$, no. 194. One hexagonal unit cell contains two formula units: K_4Te_4. The alkali-metal atoms occupy two different crystallographic sites: K1 at $2a$, $(0,0,0)$, and one aligned with the Te-Te dumbbells at $2c$, $(\frac{1}{3}, \frac{2}{3}, \frac{1}{4})$. The Te atoms are located at positions $4f$, $(\frac{1}{3}, \frac{2}{3}, z)$.

The dumbbells are still parallel to the c axis, but they no longer form chains. The structure can be built of one basic fragment, a Te-Te dumbbell followed by a K-atom parallel to the c axis. Each unit cell contains two of such basic modules at $(x,y) = (\frac{1}{3}, \frac{2}{3})$ and $(\frac{2}{3}, \frac{1}{3})$. The K atom is at the same height as the center of gravity of the dumbbell of the other module. In addition two K atoms occupy sites at the origin and at $z = c/2$. As the dumbbells are well separated from each other by the K atoms, the distance between the Te_2^{2-} dianions is increased compared to the Na_2O_2 type.

As for α-K_2Te_2 lattice parameters, volume, and excess volume are summarized in Table III. Compared to α-K_2Te_2 the error in the calculated equilibrium volume in β-K_2Te_2 is slightly increased to 3.6%. The tendency to a larger excess volume is correctly predicted, but again the excess volume is underestimated. In addition to the volume, the GGA calculation reproduces the ratio c/a. As shown in Fig. 3(b) the lattice parameters a and c both increase linearly with increasing volume.

In Table V the internal parameter z and the interatomic distances in β-K_2Te_2 are summarized. The position of the Te atom is reproduced to very high accuracy, as is the ratio of first- to second-nearest-neighbor Te-Te distances d_1^{Te-Te}/d_2^{Te-Te}. Compared to the Na_2O_2 type the second-nearest-neighbor distances are increased about 25%. The volume dependence is the same as already mentioned for the Na_2O_2 type. The dumbbell length remains unchanged [note the scale in Fig. 4(b)]. The volume effects can only be seen in the second-nearest-neighbor distances.

3. Comparison of α-K_2Te_2 and β-K_2Te_2

As far as is known, the phase transition from α-K_2Te_2 to β-K_2Te_2 is irreversible.[26,37] The relationship between the two structures is shown in Fig. 3(a).
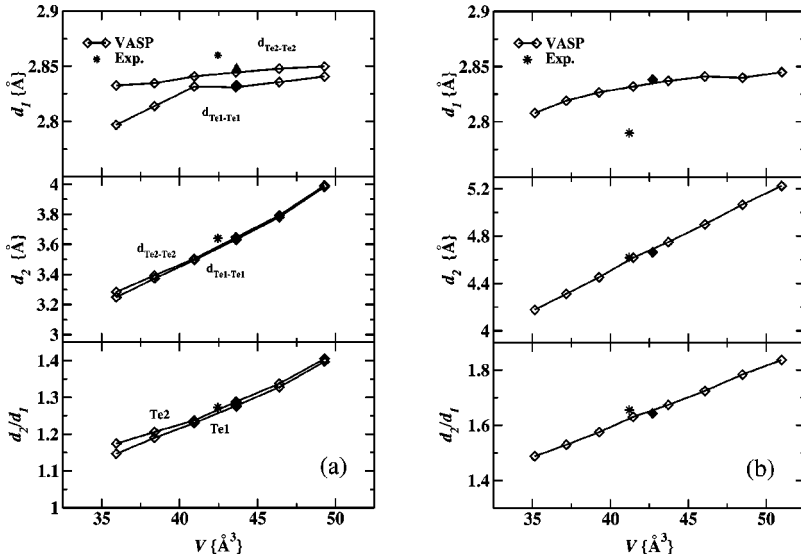
FIG. 4. Variation of the interatomic Te-Te distances over volume of (a) α-K_2Te_2 and (b) β-K_2Te_2. Filled symbols denote distances in the fully relaxed structure at equilibrium volume and stars the distances in the experimental structure.

One can relate the unit cell of the β phase to that of the α phase, with $a_\alpha \approx \sqrt{3}a_\beta$ and by doubling the unit cell of the α phase in the z direction. For a detailed discussion of the relation between the two structures, see Ref. 37. In Fig. 3(b) the lattice parameters a_α and c_α of α-K_2Te_2 are compared to the scaled parameters $\sqrt{3}a_\beta$ and $c_\beta/2$ of β-K_2Te_2. Both sets show a similar variation with volume, but at no volume in the plotted range do the two curves have the same values at the same volume. As there is no group/subgroup relation between these structures, there is no way to derive, e.g., the β phase as a high-symmetry special case from the α phase just by changing an order parameter. As Keller[37] mentioned, there is no possibility to transform the α phase into the β phase *without* breaking Te-Te bonds.

In Fig. 5 calculated energies and pressures at different volumes for both structures are fitted to the Murnaghan equation of state. The equilibrium volumes, cohesive energies, heats of formation, bulk modulus, and pressure derivative are collected in Table VI. The structural enthalpy difference at zero pressure is 1.1 meV/atom, the α phase is energetically preferred for the relaxed structure, in agreement with the observed low-temperature stability of the α phase. However, one has to admit that the calculated enthalpy difference is at the very limit of the achievable computational accuracy. For the β phase the energy of the experimental structure lies on the energy-volume curves for the relaxed structure, i.e., the relaxation at fixed volume hardly changes the total energy. The optimization of the structure of α-K_2Te_2 leads to an

significant lowering of the energy. So if we compare the energies calculated for the experimental structures, the β phase would be stable ($\Delta E \sim 17$ meV). Under a slight compression, a pressure-induced transition $\alpha \rightarrow \beta$ is predicted, in agreement with the slightly larger bulk modulus for the β phase. No experimental studies under increased pressure are known.

B. Electronic structure

In Fig. 6 the total and angular-momentum-decomposed densities of states for α- (left panel) and β-K_2Te_2 (right
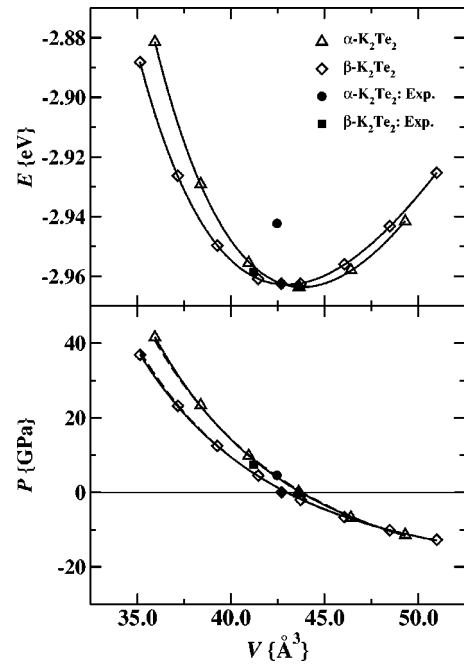
FIG. 5. Energy-volume and pressure-volume data for α-K_2Te_2 (triangles) and β-K_2Te_2 (diamonds) fitted to a Murnaghan equation of state. Filled symbols denote calculated energies and pressures for α-K_2Te_2 in the relaxed (triangle) and experimental (circle) structures and for β-K_2Te_2 in the relaxed (diamond) and the experimental (square) structure.

TABLE V. Internal parameter and interatomic distances in β-K_2Te_2 compared to experimental data.

	z	$d_1^{Te\text{-}Te}$	$d_2^{Te\text{-}Te}$	d_2/d_1
VASP	0.6350	2.838	4.664	1.643
Expt.	0.6355	2.790	4.618	1.655
		$d_{K1\text{-}K2}$	$d_{K1\text{-}Te}$	$d_{K2\text{-}Te}$
VASP		4.491	3.665	3.560
Expt.		4.438	3.625	3.515

TABLE VI. Parameters fitting the energy-volume and pressure-volume data for α– and β-K_2Te_2 to a Murnaghan equation of states by a least square fit.

	Ω_0 (Å)	E_0 (eV)	ΔH(eV)	B_0 (GPa)	B_0'
α-K_2Te_2[a]	43.818	−2.964	−0.870	12.8	4.5
α-K_2Te_2[b]	43.737	−2.964	−0.870	12.7	4.8
β-K_2Te_2[a]	42.971	−2.963	−0.869	11.1	4.9
β-K_2Te_2[b]	42.999	−2.963	−0.869	11.0	4.7

[a]Volume-energy fit.
[b]Volume-pressure fit.

panel) are shown. The partial density of states was obtained by projecting the plane waves onto the spherical harmonics within the Pauling radii ($d_{K^+} = 1.33$ Å and $d_{Te^-} = 2.21$ Å). However, whereas in β-K_2Te_2 where the Te_2 dumbbells are isolated, both s bands have a simple unimodular DOS, the interaction between the Te_2 dimers along the chains characteristic for α-K_2Te_2 leads to a DOS with pronounced van Hove singularities at the lower and upper edges. This form of the DOS is characteristic for s-bonded linear chains—this structure is more pronounced for the $ss\sigma^*$ bonds, because the antibonding states show a larger interdimer overlap. For both modifications the deep s band is split into a bonding $ss\sigma$ and an antibonding $ss\sigma^*$ part, typical for Te_2^{2-} dumb-

bells. The analysis of the partial charge densities for all s electrons confirm this characterization of the bands.

The occupied p valence states are trimerized in bonding $pp\sigma$, bonding $pp\pi$, and antibonding $pp\pi^*$ bands. According to the small distance between the dumbells the bands overlap ($pp\sigma$-$pp\pi$) or are separated by a small gap ($pp\pi$-$pp\pi^*$) in α-K_2Te_2. The $pp\sigma$ DOS is rather broad and has again a parabolic form, the upper edge overlapping with the $pp\pi$ band. The p valence bands of β-K_2Te_2 have the same characteristics as in the α phase, but now they are narrower and well separated from each other.

The density maximum of the bonding $pp\sigma$ band ($1e^-$ per atom) is located at the center of each dumbbell (see Figs. 7 and 8), $pp\sigma$ states extend at each end, leading to overlapping states centered at different dimers in the case of the α phase, but with a distinct minimum between two neighboring dumbbells for the β phase (see Figs. 7 and 8). The bonding $pp\pi$ density covers each dumbbell completely. In the case of the α phase the $pp\pi$ charge density vanishes between the dumbbells. The antibonding $pp\pi^*$ states form "doughnuts" at each end of the dumbbells, perpendicular to the c axis.

The lowest conduction bands are of $pp\sigma^*$ character, broad and parabolic and separated by a small indirect gap $\Gamma \rightarrow A$ of 0.18 eV in α-K_2Te_2. In contrast the $pp\sigma^*$ states in β-K_2Te_2 form a narrow unimodular band separated by a direct gap of 0.67 eV from the highest occupied states.
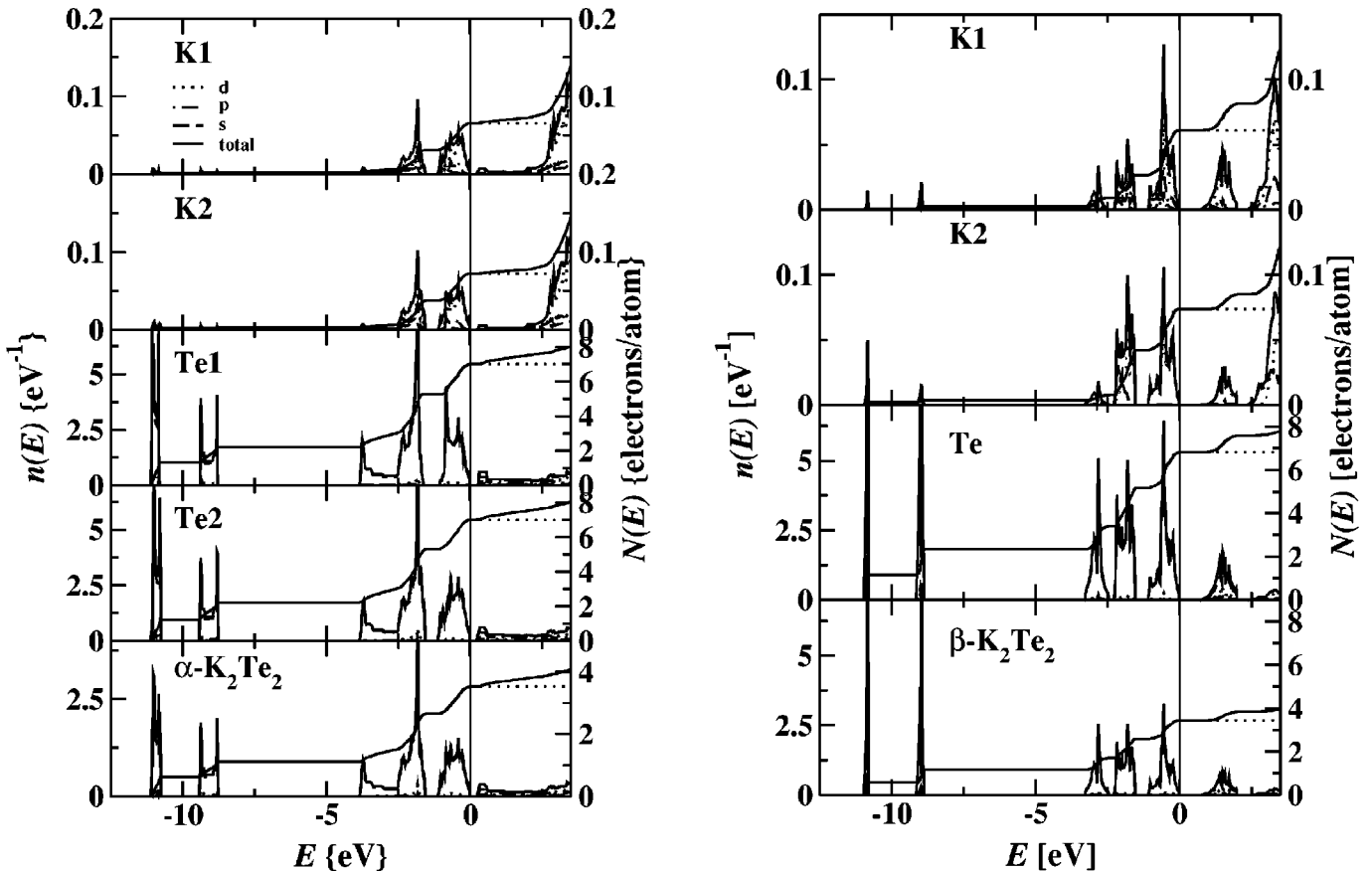
FIG. 6. Total and angular-momentum-decomposed DOS of α- (left panel) and β-K_2Te_2 (right panel). The right-hand scale refers to the integrated DOS. Please note the different scales for the K, Te, and K_2Te_2 DOS.
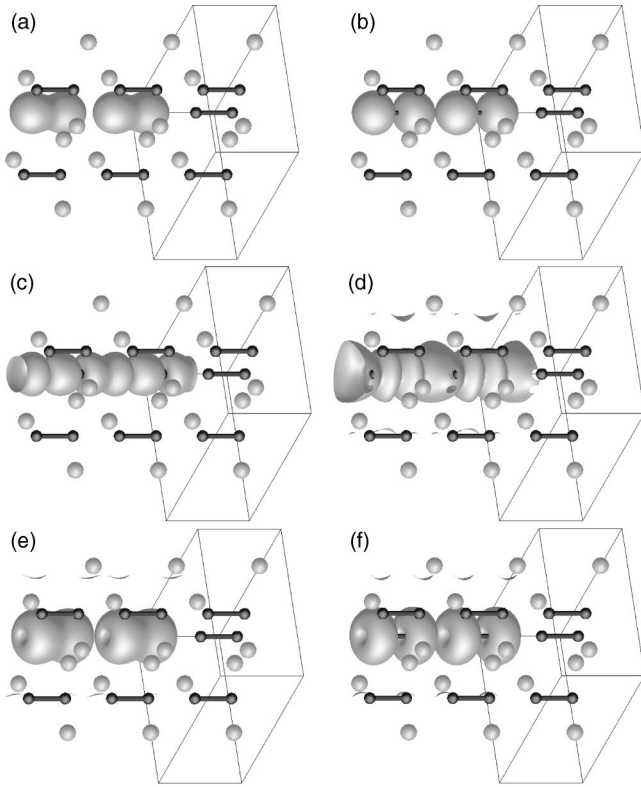
FIG. 7. Partial charge densities of α-K_2Te_2 for the (a) $ss\sigma$, (b) $ss\sigma^*$, (c) $pp\sigma$, (d) $pp\sigma^*$, (e) $pp\pi$, and (f) $pp\pi^*$ states. The light frames mark the boundaries of a unit cell.

Hence the analysis of the partial charge density (Figs. 7 and 8) leads to a picture confirming the analysis of the density of states: The chemical bonding is determined by the states of the Te_2^{2-} dumbbells leading to very similar main features in the density of states as well as in the charge
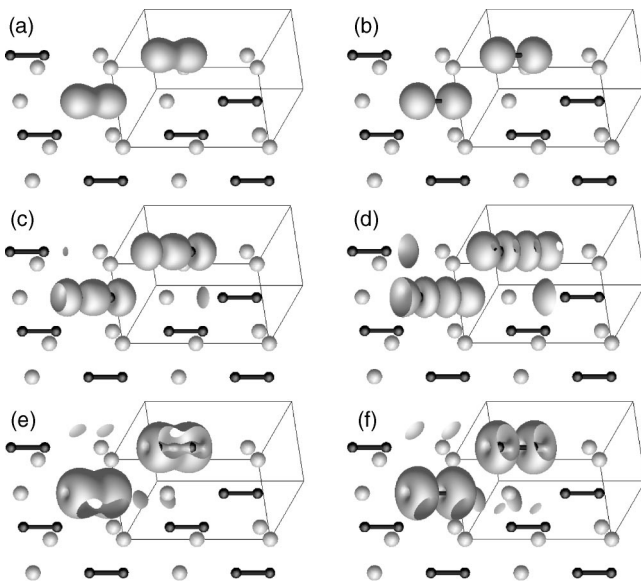
FIG. 8. Partial charge densities of β-K_2Te_2 for the (a) $ss\sigma$, (b) $ss\sigma^*$, (c) $pp\sigma$, (d) $pp\sigma^*$, (e) $pp\pi$, and (f) $pp\pi^*$ states. The light frames mark the boundaries of a unit cell.

density. In α-K_2Te_2 these dumbbells form infinite chains. The density of states and the partial charge densities indicate that two neighboring atoms from different dumbbells do not form a covalent bond, but the width and the characteristic double-peak structure of the $ss\sigma$ and $pp\sigma$ bands indicates that the interaction is not negligible. In β-K_2Te_2 the dumbbells are isolated from each other by the surrounding cations leading to sharp dispersionless bands in the density of states.

V. THE TELLURIUM ENRICHED ALLOY K_2Te_3

A. The atomic structure

K_2Te_3 crystallizes in a primitive orthorhombic lattice, space group $Pnma$, no. 62, with four formula units per cell.[27] The alkali metal is located at Wyckoff position $8d$, (x,y,z). The chalcogen atoms Te1, Te2, and Te3 occupy three crystallographically distinct sites, Wyckoff position $4c$, $(x,\frac{1}{4},z)$.

The structure has 12 free parameters to optimize (3 cell parameters, 3 for the position of the K atom, and 2 for each tellurium atom). The cell parameters are summarized in Table VII. Our calculation slightly overestimates the atomic volume, but the error is less then 2% compared to the experimental volume. The excess volume of $\Delta\Omega_{ex}\sim-25\%$ is reproduced by our calculation. The structural parameters are also reproduced to a very high degree of accuracy (see Table VII). The lattice is built of planes containing Te_3^{2-} trimers separated by rumpled K planes. In Fig. 9(a) a projection of the structure on the xy and xz planes is shown. The dark small balls denote tellurium atoms, the light big ones potassium. Te-Te nearest- and next-nearest-neighbor bonds are also shown. Te3 is always the bridging atom, bound to Te1 and Te2. These trimers are arranged in planes perpendicular to the b axis at $b/4$ and $3b/4$. The K atoms lie almost on planes between $y=0$ and $y=\frac{1}{2}$, only displaced about $\pm y, y \ll 1$. Within the layers the trimers are oriented parallel to the c axis. Along the a direction the orientation alternates (Fig. 9). The bonding lengths within the trimers are about ~ 2.8 Å (dark rods in Fig. 9). The intercluster distances $d_{Te1\text{-}Te2}$, $d_{Te1\text{-}Te3}$, and $d_{Te2\text{-}Te3}$ (light-gray rods in Fig. 9) are all between 3.5 Å and 3.7 Å, the bonding angle $\theta_{Te1\text{-}Te3\text{-}Te2}$ within the trimer is 102.0° (see also Table VII).

Agreement between theory and experiment is quite good, but we note a slight tendency to overestimate Te-Te bond lengths within the trimers, at the expense of reduced interdimer distances. To verify that the too weak covalent bond strength within the Te_3^{2-} polyanions is not due to the choice of the gradient-corrected functional, the calculations have been repeated in the LDA. We find almost the same unchanged intertrimer distances, and even smaller separation between the trimers. Hence the GGA leads to a definitely better description of the crystal structure of K_2Te_3 than the LDA. A further difference between theory and experiment concerns the significantly narrower distribution of the K-K nearest-neighbor distances resulting from the calculations. The smaller differences result mainly from a smaller y parameter for the K positions reducing the corrugation of the K planes (cf. Fig. 9). As discussed above, we suspect that due

TABLE VII. Equilibrium volume, lattice parameters, internal parameters, interatomic distances, and bonding angle within the Te_3^{2-} trimers of K_2Te_3 compared to experiment(Ref. 27).

	a(Å)	b(Å)	c(Å)	Ω(Å^3)	$\Delta\Omega$	$\Delta\Omega_{ex}$
VASP	15.952	10.343	4.645	38.3155	1.62%	−24.25%
Expt.	15.938	10.097	4.686	37.7050		−25.51%

		Internal parameters				
		VASP			Expt.	
	x	y	z	x	y	z
K1 (8d)	0.3774	0.0284	0.2867	0.3776	0.0303	0.2892
Te1 (4c)	0.4799	0.25	0.8055	0.4815	0.25	0.8152
Te2 (4c)	0.2609	0.25	0.7156	0.2594	0.25	0.7020
Te3 (4c)	0.1224	0.25	0.3121	0.1223	0.25	0.3267

		Interatomic distances (Å) and bonding angles (deg)				
	Te1-Te3[a]	Te2-Te3[a]	Te1-Te2[a]	Te1-Te3[b]	Te2-Te3[b]	Te1-Te2[b]
VASP	2.8839	2.8831	4.4823	3.6592	3.5612	3.5216
Expt.	2.8021	2.8049	4.4299	3.7528	3.6529	3.5794

	$d_{K\text{-}K}$	$d_{K\text{-}Te}$	$\theta_{Te1\text{-}Te3\text{-}Te2}$
VASP	4.6447–4.7678	3.5482–3.9830	102.0°
Expt.	4.4159–4.7899	3.4945–4.0052	104.4°

[a]Within Te_3^{2-} trimers in the (x,y) plane.
[b]Between Te_3^{2-} trimers.

to the small contributions of the K atoms to the scattered x ray intensities, the K-positions might be subject to a small uncertainty.

B. Electronic structure and chemical bonding properties

In Fig. 10 the total and angular-momentum-decomposed densities of states at the different crystal sites is shown. For

(a)

(b)
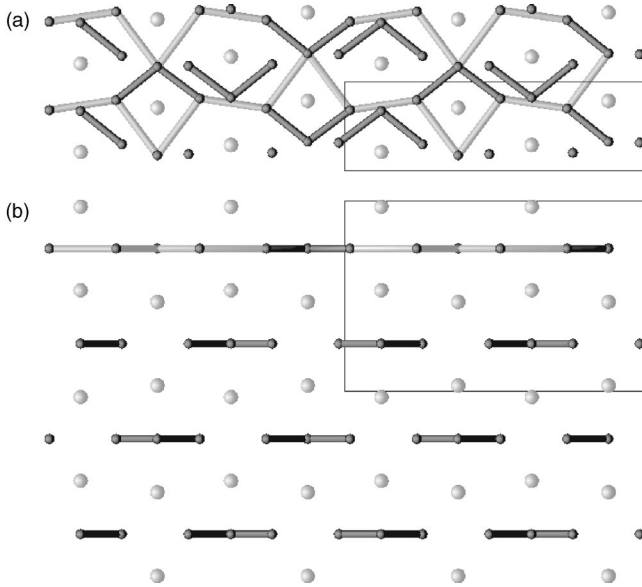
FIG. 9. The structure of K_2Te_3 projected on the (a) xz and (b) xy planes. Dark balls: Te. Light balls: K. Dark rods: shortest Te-Te distances within the Te_3^{2-} cluster. Light rods: intercluster distances. The latter are only plotted in one specific Te plane to avoid confusion. The light frames circumscribe the unit cell.

the projection spheres onto atomic spheres again the Pauli radii $R_{K+}=1.33$ Å and $R_{Te-}=2.10$ Å were chosen. The s band is trimerized, and the bonding, nonbonding, and antibonding subbands are separated by well-defined gaps. The whole s-band complex contains two electrons per tellurium atom. The largest contribution to the bonding $ss\sigma$ states comes from the bridging Te3 atom. This is also confirmed by the partial charge density [see Fig. 11(a)]. (Note that in the absence of axial symmetry for the bent trimer the designation of bonds as either σ or π is not entirely adequate. We continue to use this nomenclature, but it should be kept in mind that it refers only to the overlap of orbitals on neighboring atoms and not to the symmetry of the trimer as a whole.) The nonbonding $ss\sigma^0$ states are located at terminal atoms Te1 and Te2 only [Fig. 11(b)]. The charge density of the antibonding $ss\sigma^*$ bands is concentrated at all three Te sites with no overlap [see Fig 11(c)].

The lowest p band consists essentially of $pp\sigma$ states involving two orthogonal p orbitals on the central Te3 site, forming σ bonds with p orbitals on the terminating atoms. Therefore the electron density of this $pp\sigma$ band is mainly located around the bridging atom [see Fig 11(d)]. It contains two electrons per tellurium atom. The bonding band is separated from the nonbonding p states by a very narrow, but nevertheless recognizable gap. The second p band close to the Fermi level consists of two p orbitals perpendicular to the Te-Te bond on the terminal Te1 and Te2 sites and the remaining p orbitals perpendicular to the plane of the trimer on the central Te3 site [see Fig. 11(e)]. In terms of the orbitals perpendicular to the plane it has some π character. The orbitals centred at the terminal atoms are rather extended, leading to an appreciable overlap between neighboring trimers and to
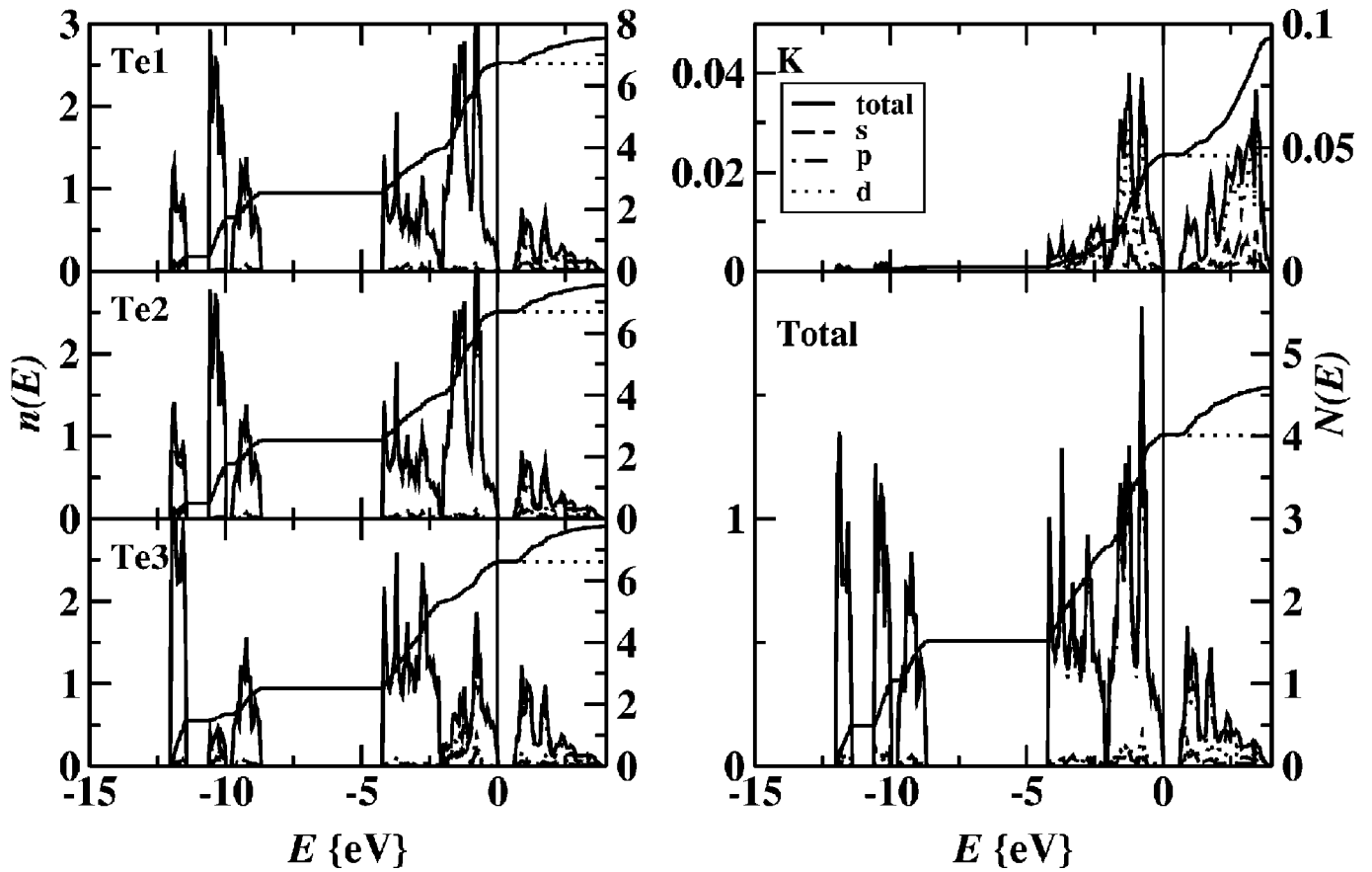
FIG. 10. Total and angular-momentum-decomposed DOS $n(E)$ (in units of states/eV atom) and integrated DOS $N(E)$ (in units of electrons/atom) of K_2Te_3. Please note the different scales for the partial K, Te, and the total K_2Te_3 DOS.
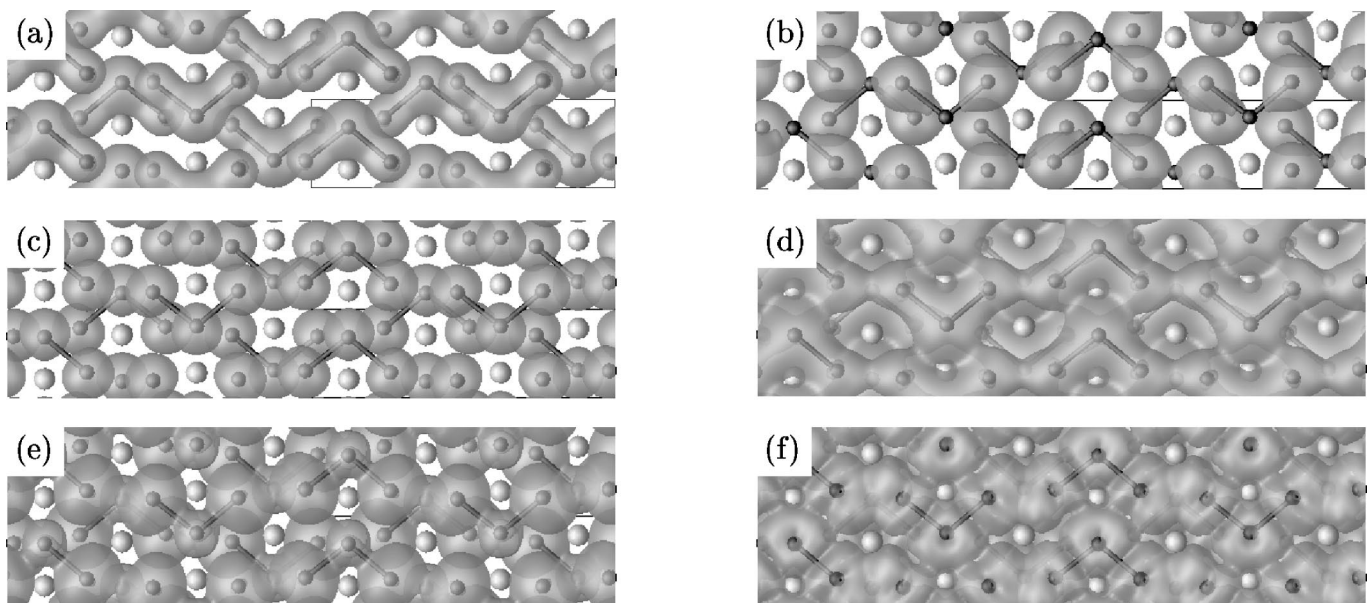
FIG. 11. Partial charge densities of K_2Te_3. Dark small spheres indicate the Te atoms, larger light ones K atoms. The dark rods mark the nearest Te-Te distances: (a) $ss\sigma$, (b) $ss\sigma^0$, (c) $ss\sigma^*$, (d) to (f) p bands (cf. text).

TABLE VIII. Equilibrium volume, lattice parameters, and bulk modulus of K_5Te_3 compared to experiment (Ref. 28).

	a(Å)	c(Å)	c/a	Ω(Å^3)	$\Delta\Omega$	$\Delta\Omega_{ex}$	B_0 (GPa)
VASP	13.8611	6.4468	0.4651	38.71	3.1%	-34.8%	14.4
Expt.	13.742	6.346	0.4631	37.56	—	-37.4%	—

the formation of zigzag chains with alternating strong intra-trimer and weak intertrimer bonds.

Projection of the partial p charge density on the xy plane would show that the regions between the Te planes are not covered; hence the charge density there is very low. The low-energy edge of the conduction band lies 0.6 eV above the Fermi energy E_F. The lowest conduction band has mainly $pp\pi$ character (see Fig. 10), however, with a certain mixed Te p–K d character as the lowering of the potassium d band, according to the high electronic pressure at the K cations, yields to an overlap of the Te and K states.

VI. POTASSIUM-ENRICHED ALLOY K_5Te_3

A. Atomic structure of K_5Te_3

K_5Te_3 crystallizes in a tetragonal lattice,[28] space group $I4/m$, no. 67. The unit cell contains 4 formula units with Te1 at Wyckoff position $4e$, $(0,0,z)$, Te2, K1, and K2 are located at Wyckoff position $8h$, $(x,y,0)$ and K3 at $4d$, $(0,\frac{1}{2},\frac{1}{4})$. The most important cell parameters are summarized in Table VIII. Agreement with experiment[28] is again reasonable: the error in the equilibrium volume is 3%. The axial ratio c/a is reproduced almost perfectly, the positions of the atoms within the unit cell (Table IX) and the interatomic distances (Table X) agree well with experiment.

The structure of K_5Te_3, as shown in Fig. 12, consists of two different basic modules: Columns of basis-sharing square antiprisms built by K atoms and centered by Te dumbbells, and columns of corner-sharing distorted (flattened) tetrahedra of Te atoms, centered by K atoms (see Fig. 12). Interatomic distances are compiled in Table X. The dumbbells located in the square-antiprismatic columns have a length of 2.853 Å, comparable to the shortest Te-Te distances in α- and β-K_2Te_2. The shortest Te2-Te2 distances are 4.9 Å between the tetrahedral columns, and 5.4 Å to 6.1 Å within the columns. This indicates that the tetrahedra are not a real building block of the structure. Assuming complete charge transfer, the chemical formula of the compound may be written as $K^+Te^-K_4^+(Te_2)^{2-}$. The Te2 sites are occupied by

TABLE IX. Internal parameters in K_5Te_3 compared to experiment (Ref. 28).

			Internal parameters				
	x_{K1}	y_{K1}	x_{K2}	y_{K2}	z_{K3}	x_{Te2}	y_{Te2}
VASP	0.2245	0.0903	0.4117	0.2806	0.2213	0.1556	0.3450
Expt.	0.2248	0.0898	0.4120	0.2804	0.2231	0.1560	0.3440

TABLE X. Interatomic distances in K_5Te_3 compared to experiment (Ref. 28).

	Within quadratic antiprismatic columns				
	$d^1_{Te1\text{-}Te1}$	$d^2_{Te1\text{-}Te1}$	$d_{K\text{-}K}$	$d_{K1\text{-}Te1}$	$d_{K2\text{-}Te1}$
VASP	2.853	3.594	3.700–4.065	3.645	3.739
Expt.	2.839	3.525	3.671–4.104	3.617	3.698

	Within tetrahedral columns			Between columns	
	$d_{Te2\text{-}Te2}$	$d_{K3\text{-}K3}$	$d_{K3\text{-}Te2}$	$d_{Te2\text{-}Te2}$	$d_{K\text{-}Te2}$
VASP	5.378	3.223	3.444	4.918	3.659–3.791
Expt.	5.334	3.182	3.420	4.825	3.626–3.758

Te^{2-} anions with a complete octet shell, whereas the Te1 sites are occupied by Te^- with a single negative charge and grouped in dianions.

The K3-K3 distance in the tetrahedral columns is remarkably short, only 3.2 Å, 30% decreased compared to elemental K. However, these short K-K distances do not represent covalent bonds between the alkali-metal atoms. The short bond length is rather imposed by static reasons: $d_{K3\text{-}K3}$ is just equal to the average between the short intra- and the longer interdimer bonds between the Te1 atoms. The K-Te distances are 3.44 Å within the tetrahedral columns and ~3.65 Å in the square-antiprismatic columns and between the columns. Projecting the structure onto the basis plane (see Fig. 12) it shows a chessboard pattern of polyanionic and simple ionic columns. The polyanionic columns are formed by the $(Te_2)^{2-}$ dianions centering square-antiprismatic K^+ columns. The ionic part of the structure consists of the Te^{2-} columns centered by K^+ ions. In Fig. 13 selected Te-Te distances within and between the columns as a function of volume are plotted. The shortest $d_{Te1\text{-}Te1}$ distance remains almost unchanged over the entire volume range, whereas all others scale linear with increasing volume.

B. Electronic structure

To calculate the angular-momentum-decomposed DOS the radii for the projection spheres were chosen such that the
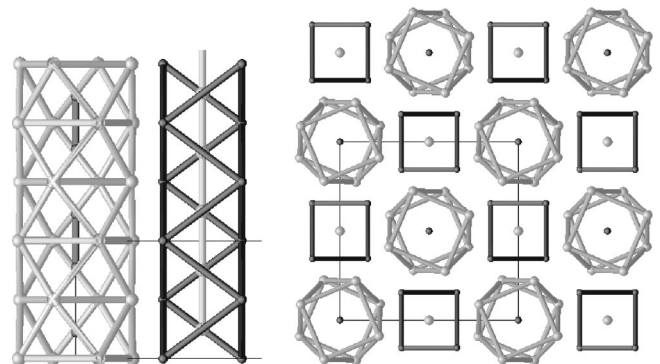
FIG. 12. Atomic structure of K_5Te_3 projected onto the xz (left panel) and the xy plane (right panel). Small dark balls: Te. Larger light balls: K. Dark rods: Te-Te distances. Light rods: K-K distances. The light frame shows the unit cell.
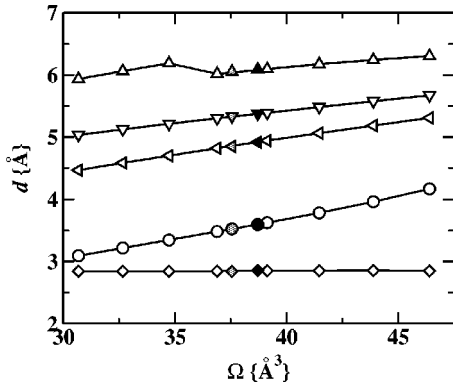
FIG. 13. Te-Te distances in K_5Te_3 at different volumes. Diamond, $d_{Te1\text{-}Te1}$ intradumbbell; circle, $d_{Te1\text{-}Te1}$ interdumbbell; left triangle, $d_{Te2\text{-}Te2}$ between tetrahedral columns; up and down triangle, $d_{Te2\text{-}Te2}$ inside the tetrahedral columns. Filled gray symbols mark the values of the experimental structure; solid ones the distances within the fully relaxed structure.

number of electrons is 23 per formula unit. The Pauling radii were not appropriate in this case. K_5Te_3 is found to be a narrow gap semiconductor with a gap of only $E_g = 0.12$ eV. However, as the DOS of the lowest unoccupied states is very low, the apparent gap detectable by spectroscopic experiments is about 2.5 eV. The DOS (Fig. 14) is determined by Te states, and the K DOS shows strongly mixed character, indicating that these are Te states overlapping into the K projection spheres.

The two different crystallographic Te sites have two different DOS. The Te2 atoms in the tetrahedral columns show the typical configuration of an isolated atom: a needlelike s band at high binding energies and a little bit broader p band just below the Fermi edge with the center of gravity at -0.52 eV. At the Te1 site the DOS is determined by the Te dianions. The s band is split into a bonding $ss\sigma$ and an antibonding $ss\sigma^*$ band. The latter is located just below the s states of the Te2 atom (see Fig. 14). Both $ss\sigma$ bands exhibit the parabolic form typical for a linear chain of atoms. Within the occupied p bands a bonding $pp\sigma$, bonding $pp\pi$, and antibonding $pp\pi^*$ band can be distinguished, in analogy to the electronic structure of $\alpha\text{-}K_2Te_2$. The low-lying $pp\sigma$ band and the $pp\pi$ band overlap; the $pp\pi^*$ states lie below the Fermi edge E_F, with the center of gravity at -0.71 eV, i.e., 0.2 eV below that of the Te2 p states. The lowest empty orbitals are the Te1 $pp\sigma^*$ states, forming a very broad band with low DOS overlapping at its upper edge with the lowest K-derived band.

Altogether the analysis of the electronic spectrum confirms the conclusion drawn on the basis of the crystal structure that K_5Te_3 may be understood as a compound formed by ionic and polyanionic elements according to the formula $(K_2Te)_2KTe$.

VII. DISCUSSION

We investigated the atomic and electronic structures of all known crystalline compounds in the K-Te system. In Table XI some of the characteristic parameters of these com-
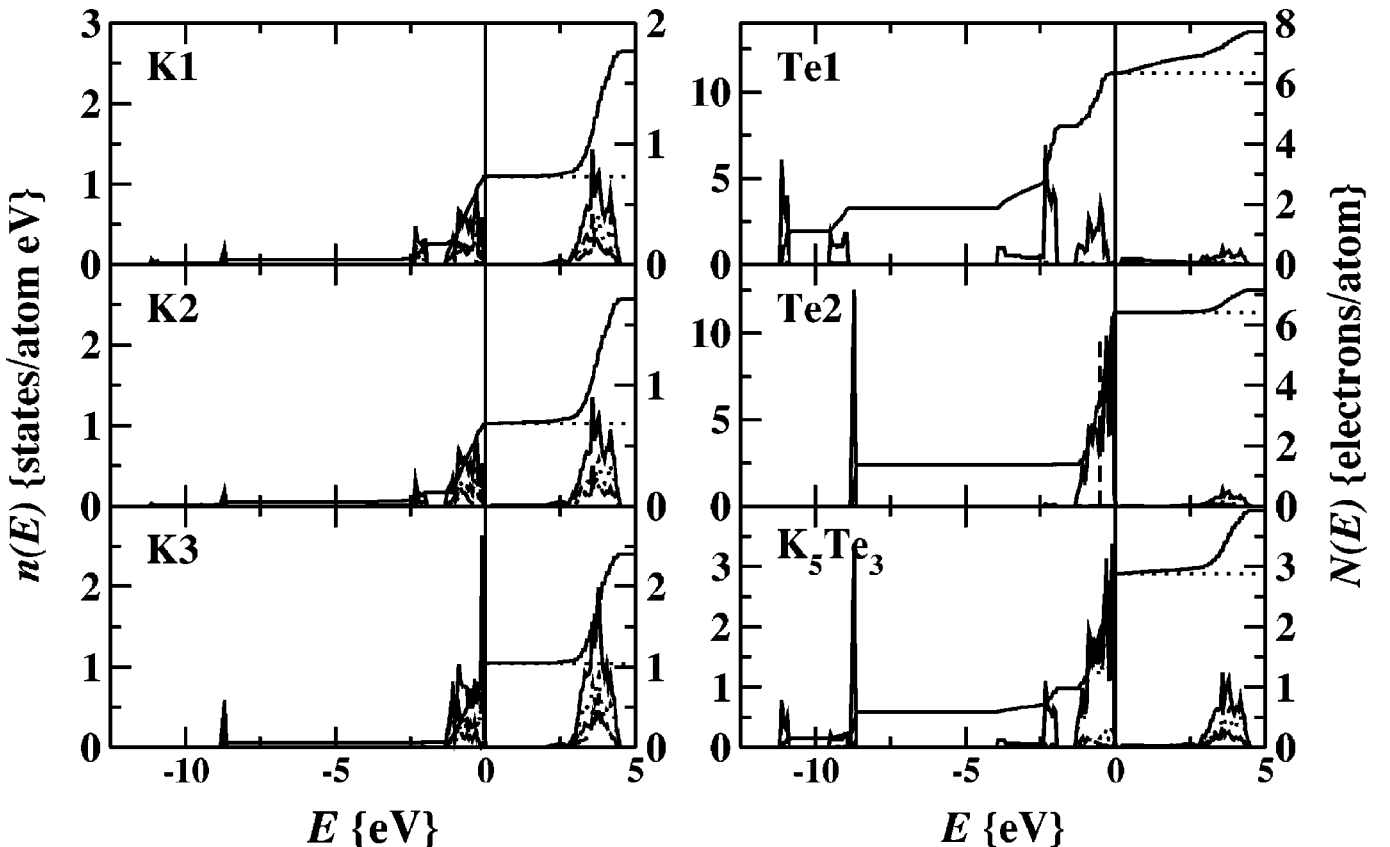
FIG. 14. Total and angular-momentum-decomposed DOS of K_5Te_3. The right-hand axis shows the integrated DOS.

TABLE XI. Equilibrium volume per atom Ω, excess volume $\Delta\Omega_{ex}$, Te-Te interatomic distances $d_{Te\text{-}Te}$, cohesive energy E, heat of formation ΔH, bulk modulus B_0, and cluster type of the crystalline compounds in the K-Te system.

System	Ω (Å^3)	$\Delta\Omega_{ex}$ (%)	$d^1_{Te\text{-}Te}$ (Å)	$d^2_{Te\text{-}Te}$ (Å	E (eV)	ΔH (eV)	B_0 (GPa)	Polyanions
K	73.96	—	—	—	−1.032	—	34.0	—
K_2Te	46.50	−23.7	—	5.82	−2.804	−1.064	12.9	Te^{2-}
K_5Te_3	38.71	−34.8	2.85	3.59	−2.831	−1.003	14.4	$(Te_2)^{2-}$, Te^{2-}
α-K_2Te_2	43.66	−19.9	2.83	3.65	−2.964	−0.870	12.7	$(Te_2)^{2-}$
β-K_2Te_2	42.70	−21.6	2.84	4.66	−2.963	−0.869	11.1	$(Te_2)^{2-}$
K_2Te_3	38.32	−24.2	2.88	3.52	−3.050	−0.744	14.3	$(Te_3)^{2-}$
Te	35.00	—	2.89	3.50	−3.156	—	19.4	—

pounds, including elemental K and Te under standard conditions, are summarized. Pure K is a simple metal, the structure being determined by packing requirements. Te, on the other hand, is a semiconductor consisting of helical chains of Te atoms, each of them having two covalently bonded neighbors. The crystal structure of trigonal Te is the result of a Peierls distortion leading to a trimerization of the 2/3 filled Te p band. The compounds in the K-Te system are first of all determined by the large difference in the electronegativity between the two components. Table X summarizes the calculated results for the equilibrium volume, excess volume, nearest- and next-nearest Te-Te distances, cohesive energy, heat of formation, and bulk moduli. Figure 15 shows the heat of formation ΔH as a function of composition. We see immediately that the saltlike compound K_2Te has the highest ΔH, and the heats of formation of the polyanionic (or partially polyanionic) compounds with higher Te content lie almost on the straight line connecting $\Delta H(K_2Te)$ and $\Delta H = 0$ for pure Te. Hence all the compounds have comparable stability. Only for K_5Te_3 the calculated heat of formation is found to be not sufficiently exothermic by about ~20 meV/atom, which explains its instability towards decomposition into K_2Te and K_2Te_2.

The stoichiometric phase K_2Te is a typical saltlike compound, the ions being arranged in a closed-packed fcc struc-
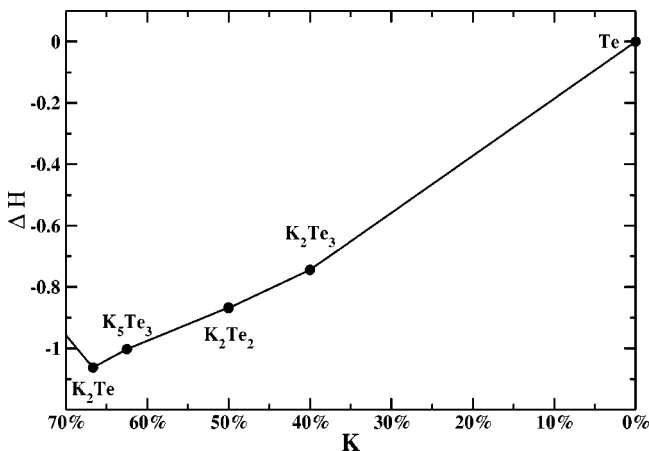
FIG. 15. Heat of formation of the different phases in the K-Te system.

ture. The Te^{2-} anions have the octet configuration $[Kr]4d^{10}5s^25p^6$ and occupy the octahedral holes in the K^+ matrix. The K^+ cations have the same electronic configuration as Ar. The large excess volume can be explained by the decrease of the K radius upon ionization.

In the potassium-rich compound K_5Te_3 there are too few electrons, given by the K atoms, to obtain an octet configuration for *all* Te atoms, so that 1/3 of the Te atoms become isoelectronic only to iodine, building $(Te_2)^{2-}$ dumbbells, in analogy to iodine molecules. The structure as described in Sec. VI A reflects the two types of Te cations. The $(Te_2)^{2-}$ dianions are centered inside columns built of K^+ cations; the Te^{2-} anions build columns centered by a chain of K^+ cations. The K-K distance within these chains is remarkably short. The excess volume is $\sim10\%$ larger than the excess volumes in all other compounds in the K-Te system. This cannot be explained only by the decreased K^+ radius. As shown in Table XI the Te-Te bond length in all compounds except K_2Te, where there were no direct Te-Te neighbors, are comparable. Hence the dimension of the square-antiprismatic columns of K ions are determined by the length of the Te dumbbells along the c axis. The short K-Te distances of $d_{K\text{-}Te}=3.645$ Å and 3.739 Å between the K^+ cations of the square-antiprismatic columns and the Te^{2-} anions of the tetrahedral columns indicate a certain degree of ionic bonding between the different building blocks. The distances set by the Te-Te bonds in the dumbbells determine via the coupling of the K^+ cations and the Te^{2-} cations also the dimension of the tetrahedral columns leading to the surprisingly short K-K distances and the large excess volume of this crystalline phase. As already stressed in Sec. VI B the electronic density of states reflects also the ionic character of the bonding between the two elements and the different character of the Te ions at the different crystallographic sites.

Both crystalline phases of the equiatomic compound are classical Zintl-Klemm alloys. Both build $(Te_2)^{2-}$ dumbbells. The arrangement of these dianions within the K^+ matrix differs: In α-K_2Te_2 the dianions build infinite straight chains with alternating short and long distances. As shown in Table XI these nearest- and next-nearest-neighbor distances have similar lengths as the first two distances in trigonal Te. In β-K_2Te_2 the dumbbells are isolated from each other by the K^+ matrix, the next-nearest Te-Te distance is increased by about

1 Å. The equilibrium volume of the β phase is a bit smaller than that of the α-phase. The Zintl principle gives us a heuristic explanation: As the Te_2^{2-} dumbbells carry two negative charges, there exists a repulsive Coulomb potential between the dumbbells. In the β phase this potential is more efficiently screened by the surrounding alkali-metal atoms, allowing a tighter packing than in the α phase. The difference in the atomic structure can also be seen in the electronic DOS: Both phases are characterized by a double-peak structure of bonding and antibonding states, but the $ss\sigma$, $ss\sigma^*$, and the $pp\sigma$ bands of the α phase show in addition the parabolic form characteristic for a linear chain of atoms. This leads to slightly lowered centers of gravity within the s and p bands compared to those of β-K_2Te_2. α-K_2Te_2 is energetically preferred, but transforms into the β phase under compression and at elevated temperature (although finite T is not considered here).

The structure of the tellurium-rich compound K_2Te_3 is another example for the flexibility of the Zintl principle: Due to the charge transfer from the potassium atom to the tellurium, each tellurium atom has $6+\frac{2}{3}$ electrons. To obtain an octet configuration three atoms have to share $3\times6+2$ electrons; hence they build trimers with an bond angle of $\sim100°$ as a transition structure to the infinite chains in t-Te. The trimers are arranged in a plane, each of these planes being separated by layers of K^+ atoms.

All compounds in the K-Te system have a remarkably large negative excess volume, being largest in K_5Te_3 with -34.8%. The excess volumes of all other compounds are in the range of ~20–25%. In all cases the calculated excess volumes are always slightly smaller than those found experimentally. As the volume contraction is mainly due to the small ionic radius of of the potassium and the strong covalent bonding in the polyanions, the error arises from the underestimation of the volume of pure potassium.

VIII. CONCLUSIONS

All crystalline phases in the K-Te system confirm the validity of a generalized Zintl picture. In K_2Te the Te^{2-} ions have an octet configuration forming a saltlike compound, with isolated anions surrounded by the cations. At reduced K content, an octet shell cannot be completed for all Te atoms and the Te anions are forced to build polyanionic clusters. At the stoichiometry 1:1 Te forms Te_2^{2-} dumbbells, comparable to the I_2 molecule in crystalline iodine. Two different phases are found at this composition. In both phases the main module is the Te_2^{2-} dumbbell, but in case of the α phase they are arranged in an infinite straight chain with alternating short

and long Te-Te distances whereas in the β phase they are isolated within a potassium matrix. In K_5Te_3, a fraction of the Te atoms can acquire a octet shell, whereas others become isoelectronic only to iodine. The resulting structure is a mixture of ionic and polyanionic elements. Finally in K_2Te_3 the tellurium atoms form trimers arranged in a planar network with strong Te-Te bonds within and weak bonds between the trimers, each plane being separated by layers of potassium atoms. This structure may be viewed as intermediate between the polyanionic phase based on Te dumbbells and the chainlike structure of elemental Te. Going from the potassium-rich end of the K-Te system towards trigonal Te the tendency to form polyanionic structures increases: From K_2Te where the structure has dimension 0 (isolated Te^{2-} ions), over the linear $(Te_2)^{2-}$ dianions in K_5Te_3 and α-K_2Te_2 (one-dimensional) to the layers of $(Te_3)_2$ trimers in K_2Te_3 (two-dimensional) and to the three-dimensional helical chains in trigonal tellurium.

The K-Te system is not the only one where a wide variety of Zintl phases with different valence electron concentrations may be found. Other examples are K-Sb and Li-Ga. In K-Sb, a saltlike compound K_3Sb coexists with a polyanionic phase KSb (where the Sb atoms form infinite spiral chains resembling the structure of t-Te) and an electron-excess compound K_5Sb_4 in which the extra electrons provided by the added K atom serve to saturate the dangling bonds at the ends of zigzag shaped tetramers. In Li-Ga the equiatomic compound $LiGa$ with the NaTl ($B32$) structure is a classical Zintl phase with Ga arranged on a diamond-type sublattice.[38] In the Li-enriched compounds Li_3Ga_2 and Li_2Ga the equivalences $Ga^{2-}\equiv As$ and $Ga^{3-}\equiv Se$ are reflected by the As-like, and Se-like, respectively, Ga sublattices and in an As-like, and Se-like, respectivey electronic spectrum. However, in this system the electronegativity difference between Li and Ga is not large enough to reach the ionic end of the structural spectrum. The K-Te compounds studied offer the most complete evidence for the flexibility of the Zintl-Klemm picture, covering the entire range from alkali-metal-rich phases to compounds enriched in the polyanionic element.

In K-Sb, Li-Ga, and other Zintl phases the Zintl-Klemm principle also determines the short- and medium-range order and the electronic properties of the molten alloys. A forthcoming paper will be devoted to an *ab initio* molecular-dynamics study of molten K-Te alloys.

[1] E. Zintl and G. Brauer, Z. Phys. Chem. Abt. A **20**, 241 (1933).

[2] E. Zintl, J. Goubeau, and W. Dullenkopf, Z. Phys. Chem. Abt. A **154**, 1 (1931).

[3] W. Hückel, *Structural Chemistry of Inorganic Compounds* (Elsevier, Amsterdam, 1951), Vol. II, p. 83.

[4] I. Hewaidy, E. Busmann, and W. Klemm, Z. Anorg. Allg. Chem. **328**, 283 (1964).

[5] R. Marsh and D. Shoemaker, Acta Crystallogr. **6**, 157 (1953).

[6] K. Seifert-Lorenz and J. Hafner, Phys. Rev. B **59**, 829 (1999).

[7] R. Xu, P. Verkerk, W.S. Howells, G.A.d. Wijs, F.v.d. Horst, and W. van der Lugt, J. Phys.: Condens. Matter **5**, 9253 (1993).

[8] *Chemistry, Structure, and Bonding of Zintl Phases and Ions*, ed-

ited by S. Kauzlarich (VCH, New York, 1996).

[9] R. Winter, in *Thermodynamics of Alloy Formation*, edited by Y. Chang and F. Sommer (The Minerals, Metals and Materials Society, London, 1997).

[10] T. Asada, T. Jarlborg, and A. Freeman, Phys. Rev. B **24**, 510 (1981); **24**, 857 (1981).

[11] D. Ellis, G. Benesh, and E. Byron, Phys. Rev. B **16**, 3308 (1977).

[12] A. Zunger, Phys. Rev. B **17**, 2582 (1978).

[13] F. Springelkamp, R. de Groot, W. Geertsma, W. van der Lugt, and F. Mueller, Phys. Rev. B **32**, 2319 (1985).

[14] M. Tegze and J. Hafner, Phys. Rev. B **39**, 8263 (1989).

[15] M. Tegze and J. Hafner, Phys. Rev. B **40**, 9841 (1989).

[16] G. Kresse, J. Furthmüller, and J. Hafner, Phys. Rev. B **50**, 13 181 (1994).

[17] M. Cohen and J. Chelikowsky, *Electronic Structure and Optical Properties of Semiconducters* (Springer, Berlin, 1988).

[18] W. van der Lugt, J. Phys.: Condens. Matter **8**, 6115 (1996).

[19] W. van der Lugt and P. Verkerk, Plasmas and Ions **3**, 3 (2000).

[20] K. Seifert-Lorenz and J. Hafner, Phys. Rev. B **59**, 843 (1999).

[21] O. Genser and J. Hafner, J. Non-Cryst. Solids **250-252**, 236 (1999).

[22] O. Genser and J. Hafner, J. Phys.: Condens. Matter **13**, 959 (2001).

[23] O. Genser and J. Hafner, J. Phys.: Condens. Matter **13**, 981 (2001).

[24] O. Genser and J. Hafner, Phys. Rev. B **63**, 144204 (2001).

[25] E. Zintl, A. Harder, and B. Dauth, Z. Elektrochem. **40**, 588 (1934).

[26] P. Böttcher, J. Getzschmann, and R. Keller, Z. Anorg. Chem. **619**, 476 (1993).

[27] B. Eisenmann and H. Schäfer, Z. Elektrochem. Angew. Phys. Chem. **90**, 731 (1978).

[28] I. Schewe and P. Böttcher, Z. Naturforsch. B **45B**, 417 (1990).

[29] Y. Wang and J.P. Perdew, Phys. Rev. B **44**, 13 298 (1991).

[30] D. Vanderbilt, Phys. Rev. B **41**, 7892 (1990).

[31] G. Kresse and J. Hafner, J. Phys.: Condens. Matter **6**, 8245 (1994).

[32] W. Press, B. Flannery, S. Teukolsky, and W. Vetterling, *Numerical Recipes* (Cambridge University Press, New York, 1989).

[33] A. Eichler, J. Hafner, J. Furthmüller, and G. Kresse, Surf. Sci. **346**, 300 (1996).

[34] P. Villars and N. Calvert, *Pearson's Handbook of Crystallographic Data for Intermetallic Phases* (American Society for Metals, Metals Park, Ohio, 1990).

[35] R. Keller, W. Holzapfel, and H. Schulz, Phys. Rev. B **16**, 4404 (1977).

[36] M. Tegze and J. Hafner, J. Phys.: Condens. Matter **3**, 2449 (1992).

[37] R. Keller, Ph.D. thesis, Universität Aachen, 1986.

[38] W. Jank and J. Hafner, Phys. Rev. B **44**, 11 662 (1991).